Original Research Article: full paper

(2022), «EUREKA: Physics and Engineering»
Number 1

THE EFFECT OF MILLING TIME ON THE ALUMINA PHASE TRANSFORMATION IN THE AMCs POWDER METALLURGY REINFORCED BY SILICA-SAND-TAILINGS

Sukanto✉
Politeknik Manufaktur Negeri Bangka Belitung
Kawasan Industri Airkantung, Sungailiat, Bangka, Indonesia, 33211
Department of Mechanical Engineering[1]
sukanto@polman-babel.ac.id

Wahyono Suprapto
Department of Mechanical Engineering[1]

Rudy Soenoko
Department of Mechanical Engineering[1]

Yudy Surya Irawan
Department of Mechanical Engineering[1]

[1]*Brawijaya University*
167 Jl. Mayjend Haryono, Malang, Indonesia, 65145

✉**Corresponding author**

Abstract

This study aims to determine the effect of milling time and sintering temperature parameters on the alumina transformation phase in the manufacture of Aluminium Matrix Composites (AMCs) reinforced by 20 % silica sand tailings using powder metallurgy technology. The matrix and fillers use waste to make the composites more efficient, clean the environment, and increase waste utilization. The milling time applied to the Mechanical Alloying (MA) process was 0.5, 6, 24, 48, and 96 hours, with a ball parameter ratio of 15:1 and a rotation of 93 rpm. Furthermore, hot compaction was carried out using a 100 MPa two-way hydraulic compression machine at a temperature of 300 °C for 20 minutes. The temperature variables of the sintering parameter process were 550, 600 to 650 °C, with a holding time of 10 minutes. Characterization of materials carried out included testing particle size, porosity, X-Ray Diffraction (XRD), SEM-Image, and SEM-EDX. The particle measurement of mechanical alloying processed, using Particle Size Analyzer (PSA) instrument and based on XRD data using the Scherrer equation, showed a relatively similar trend, decreasing particle size occurs when milling time was increased 0.5 to 24 hours. However, when the milling time increases to 48 and 96 hours, the particle size tends to increase slightly, due to cold-weld and agglomeration when the Mechanical Alloying is processed. The impact is the occurrence of the matrix and filler particle pairs in the cold-weld state. So, the results of XRD and SEM-EDX characterization showed a second phase transformation to form alumina compounds at a relatively low sintering temperature of 600 °C after the mechanical alloying process was carried out with a milling time on least 24 hours.

Keywords: mechanical alloying, milling time, powder metallurgy, AMCs, silica sand tailings, alumina.

DOI: 10.21303/2461-4262.2022.001906

1. Introduction

AMCs products have been widely applied in the aerospace and automotive industries due to their high strength-to-weight ratio [1], even aluminium metal is the second light metal after magnesium which is most widely used in industry after iron [2, 3]. The reinforcement of composite materials using a soft and ductile aluminium matrix, combined with rigid ceramic particles, such as oxides, carbides, borides, and nitrides, requires adequate engineering processes to obtain AMCs products with mechanical properties, such as lesser porosity, higher hardness, and greater resistance to friction [4–6].

Mechanical Alloying (MA) involves the mixture of matrix material and reinforcing powder as well as the simultaneous reduction of particle sizes using high-energy ball milling [7]. Therefore, MA is an essential process of powder metallurgy techniques widely used and developed as

reported in several recent studies. This solid-state method [8], involves repeated ball collisions, thereby leading to deformation, cold welding, fracturing, and re-welding of powder particles in a high-energy ball mill [9]. However, it has been widely used, to synthesize various materials, such as intermetallic compounds [10], amorphous alloys [11], nanocrystalline substances [12], carbides [13], nitrides, and composites [14].

In certain conditions, the presence of an alumina phase (Al_2O_3) in the composite product is desirable. This is based on the fact that alumina has better mechanical properties than the reinforcing metal oxides (M), such as silicon dioxide (SiO_2), iron oxide (Al_2O_3), zinc oxide (ZnO), etc. A transformation reaction synthesizes aluminium with a suitable metal oxide during the MA process under a specific sintering temperature to produce the Al_2O_3 phase based on the following equation [15]:

$$3MO + 2Al = Al_2O_3 + 3M. \quad (1)$$

The use of MA methods proposed by Radial Ball Mill technology involves a combination of the powder mixing process with the matrix, regarded as an alloying element. Conversely, when a higher level of the Al_2O_3 phase is required, an increased % wt. of M needs to be conferred to improve the material properties. Therefore, to optimize the AMCs properties, the adequacy of M needs to be determined, in addition to composing the ceramic reinforcement, the matrix also has to be designed [16]. Silicon dioxide (SiO_2) is a possible candidate for producing these AMCs because its reaction with Al produces high negative free energy (ΔG) changes [17]. The Al matrix dissolves the reduced Si, thereby increasing the mechanical properties of the composite. Several studies have been carried out on AMCs using different MA milling times [15] and sintering parameters to produce the alumina phase in the composite products. Some of these studies used Aluminium and SiO_2 material constituents with a milling time of 8 hours and sintering at 650 °C for 2 hours [18]. Furthermore, Al and ZnO materials were used with a milling time of 60 hours and sintering at 550 °C for 3 minutes [15], as well as Al, SiO_2, and C materials with a milling time of 50 hours and sintering at 650 °C for 1 hour [19].

The MA process reduces particle size, resulting in Schottky defects and Frenkel defects [20, 21], so the interstitial or substitution between particles occurs and increases the distribution of reinforcing powders across the aluminium matrix, thereby enhancing the yield strength of the AMCs constituent powders following the Hall-petch strengthening analysis [22, 23]. It also improves matrix properties, through high deformation rates, optimizes heat energy absorption and dislocation densities, including reinforcement by oxide dispersions [24]. Therefore, the MA processes involving Al-SiO_2 reduces transformation reaction temperatures below 750 °C, relatively less than that of the normal reaction, which is approximately 1000 to 1300 °C [18]. This is because the ball milling process triggers the formation of nano-sized diffusion pairs of Al-SiO_2 and accelerates associated reactions by reducing atomic diffusion distance. Besides, severe plastic deformations tend to cause significant crystal imperfections in the particles, increase the absorption of heat energy, chemical reactivity, and atomic diffusivity [25].

Previous studies used essential composites ingredients that have relatively high purity, >98 %. Meanwhile, it is generally expensive to obtain highly purified silica [26]. Likewise, the cost to produce primary aluminium is prohibitive, because it requires 95 % of the waste recycling process, thereby making AMCs expensive [3, 27]. Therefore, this research aims to produce Al-Si or Al_2O_3 micro composites using aluminium recycled materials and silica sand tailings with low purity levels (<90 %), which are relatively inexpensive. Irrespective of the fact that several preliminary studies have been carried out on the relatively high level of parameter complexity in the MA process as well as the different purposes and AMCs constituent materials used, in-depth research needs to be conducted to determine the effect of milling time and sintering temperature on the occurrence of phase transformation reactions using Al_2O_3 and AMCs fabricated with silica sand tailings reinforcement.

2. Materials and methods

2. 1. Materials

The aluminium powder used as a matrix was obtained by recycling motorcycle waste materials, namely, pulley, piston, machine block, and beverage-can packages. This process involves

a metal casting method with ingot moulds, turned into chips, using a ball mill machine [28]. The recycled aluminium casting process and the ball mill technique were carried out in the αβγ Laboratory, Landungsari, Malang, Indonesia. The aluminium produced from the recycled material is referred to as Al-ZnSiFeCuMg. Meanwhile, silica sand tailings are derived from mining and leaching waste from PT. Timah, Tbk. in Mentok, Province of Bangka-Belitung Islands, was used as reinforcement.

The size of the utilized Al-ZnSiFeCuMg and silica sand tailings material powder bases determined using PSA machines is D50: 204 μm, and D50: 31 μm respectively. The 2 powdered materials that constitute the AMCs have undergone the initial grinding process. The SEM images illustrating the dimensions and physical forms of Al-ZnSiFeCuMg and silica sand tailing powders are shown in **Fig**. **1, *a*, *b***. Meanwhile, the chemical compositions of the Al-ZnSiFeCuMg material powder base were determined using the Spectro Spark Analyzer test at PT.HP. Metal in Ngoro Industry Persada East Java Indonesia is shown in **Table 1**.

Furthermore, the chemical compositions of silica sand tailing powder base determined using the XRD test carried out at the Mineral and Advanced Materials Laboratory of the State University of Malang is shown in **Table 2.** The silica sand tailing contains several impurities due to the presence of a lesser wt. % Cu(FeO_2), and Fe_2O_3 [1].

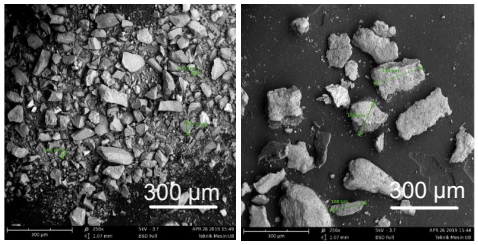

a *b*

Fig. 1. Scanning Electron Microscope (SEM) image: *a* – Powder of Al-ZnSiFeCuMg Aluminium; *b* – Powder of Silica Sand Tailings

Table 1

Chemical Composition of Al-ZnSiFeCuMg Powder [D50:204 μm]

Element	Al	Zn	Si	Fe	Cu	Mg	Sn	Pb	Sb	Ni	Other
[%]	83.15	6.16	4.35	2.20	1.30	1.13	0.37	0.33	0.28	0.16	0.56*
STDEV**	1.33	1.07	0.35	0.20	0.09	0.08	0.04	0.01	0.03	0.02	0

**Cr/Mn/Ti/Zr/Ca/Bi/Na/P/Sr/Be/Cd.*
***STDEV = Standard Deviation*

Table 2

Chemical Composition of Silica Sand Tailing Powder [D50:31 μm]

No.	Compound Name	Chemical Formula	Perct. [%]
1	Quartz	SiO_2	81
2	Maghemite	Fe_2O_3	12
3	Anatase	TiO_2	5
4	Zirconium Oxide	ZrO_2	2

2. 2. Experimental Procedure and Methods

Powder metallurgy was used to produce AMCs reinforced with silica sand tailings. This technique involves several stages, namely powder preparation and additives, blending or mixing, compaction, lubrication removal, sintering, process, and product finishing [29, 30]. The experimental procedures and methods are shown in **Fig. 2**. Schematic of Powder Metallurgy Stages on the Manufacturing AMCs Reinforced Silica Sand Tailing.

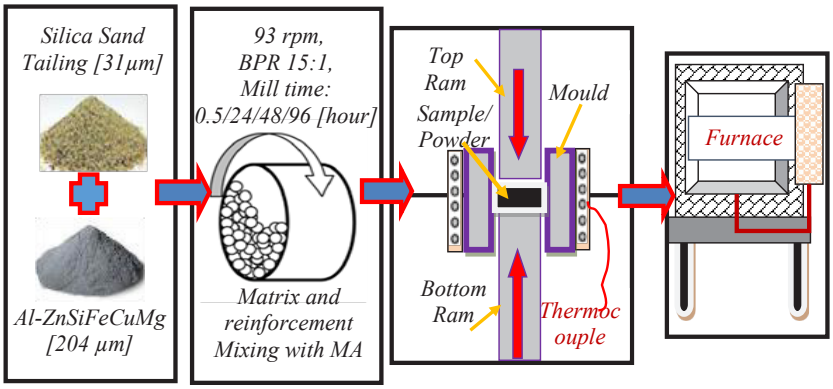

Fig. 2. Schematic of Powder Metallurgy Stages on the Manufacturing Aluminium Matrix Composites (AMCs) Reinforced Silica Sand Tailing

Generally, the extremely small reinforcement percentage used failed to provide the required strengthening effect. In contrast, the higher the percentage of the reinforcement, the easier the agglomeration thereby, making it difficult to obtain a homogeneous composites constituent mixture. Therefore, the applied matrix and reinforcement weight ratio is 80 % wt. Al-ZnSiFeCuMg and 20 % wt. silica sand tailing, SiO_2 [28, 31–33]. To achieve a thickness of ±8 mm, 25 grams of cold-weld powder from the MA process was inserted into one of the mould specimens.

The mixing of powdered AMCs constituents was realized using Mechanical Alloying with a radial Ball Mill Machine. A Ball Parameter Ratio (BPR) of 15:1 and a machine ball mill rotation of 93 revolutions per minute (rpm) were utilized [34]. The vial tube and the ball miller material were made from stainless and chrome steel, respectively. The applied milling time variations were 0.5 hours, 6 hours, 24 hours, 48 hours, and 96 hours. The MA and sintering processes were carried out using the atmosphere [35].

Furthermore, a hot-compaction system at a temperature of 300 °C, and pressure of 100 MPa for 10 minutes was utilized [30]. This mechanism used a 2-way hydraulic pump consisting of top and bottom rams. The mould specimens were ring-shaped, with outer and inner diameters of 40 mm, and 17 mm, and a thickness of 8 mm [36]. The sintering process is performed 20 days (480 hours) after the hot-compaction process was carried out to obtain a relatively stable specimen because powder metallurgy product that naturally ages within 2000 hours changes the microstructure [37]. Additionally, the rate of change in the chemical composition of the particles in the specimen is still ongoing. However, it is relatively gradual and slow.

According to [38], the reaction between Al and SiO_2 powders using the Mechanical Alloying process at a milling time of 4 hours and sintered within a temperature range of 560 and 680 °C led to a transformation reaction namely Al_2O_3. Meanwhile, composite wetting conditions of aluminium powder metallurgy generally occur at sintering temperatures of 550 and 620 °C, using a mixer or a mechanical alloying process [26]. [18], stated that smaller particle sizes produced by the MA ball-mill increase the reactivity of the composite constituent powder and the heat energy absorption efficiency, thereby causing the alumina transformation reaction to occur at a reduced temperature, of relatively 530 and 680 °C. An exothermic reaction occurs between the liquid solids Al and SiO_2. Therefore, the sintering temperature process was carried out at 550 °C, 600 °C, and 650 °C, at a holding time of ±10 minutes.

The theoretical density of the matrix and the AMCs reinforcing powder mixture is determined using the following (2) [28]:

$$\rho_T = \frac{\sum \%u \cdot \rho_u}{100} = \frac{\%u_1 \cdot \rho_{u1} + \%u_1 \cdot \rho_{u2} + \ldots + \%u_n \cdot \rho_{un}}{100}, \quad (2)$$

where, the variables of ρ_u and $\%u$ are the densities and chemical elements percentages, while ρ_T is the theoretical density value. Measurement of the density value was performed by applying

Archimedes' principle, after the hot-compaction ($\rho_{H\text{-}C}$) and sintering process (ρ_S) [39]. Initially, the density of the produced AMCs specimens, ρ_{AMCs} involved the weight of a specimen basket in water (W_{sb}), the scale weight in the air (W_a), the weight of the basket in water (W_b), and the weight of the specimen in water ($W_c = W_{sb}–W_b$). However, assuming ρ_w is the density of water, the value of the composite specimen is obtained using (3) [28]. Subsequently, the percentage porosity (γ%), of hot-compaction and sintered AMCs, were determined using (4).

$$\rho_{AMCs} = \frac{W_a}{W_a - (W_{sb} - W_b)} \times \rho_w, \tag{3}$$

$$\gamma(\%) = \frac{\rho_T - \rho_{Composite}}{\rho_T} \times 100. \tag{4}$$

The process of characterizing powdered and AMCs specimens involves the use of several instruments. First, the chemical composition of powdered materials was tested using the X'Pert Pro, Pan Analytical X-Ray Diffraction (XRD) type at the Laboratory of Minerals and Advanced Materials, State University of Malang. Meanwhile, the chemical composition of AMCs products was tested using Xpert-3 type PANanalytical X-Ray Diffraction (XRD) at the Central Laboratory of Biosciences Brawijaya University (LSIH-UB). XRD analysis was carried out using HighScore Plus software. Measurement of particle size distribution was performed using a Cilas 1090 Dry Laser Particle Size Analyzer (PSA) machine at the Chemical Engineering Laboratory of Brawijaya University. Meanwhile, microstructure analysis was carried out, using a Scanning Electron Microscope (SEM) of the FEI Quanta FEG 650 series and FE-SEM type. Besides, the elemental composition analysis was obtained using the X-act Oxford Instrument EDS detector at the Bioscience Central Laboratory of Brawijaya University (LSIH-UB).

In addition, to confirm the PSA testing carried out using the Cilas 1090 Dry PSA machine, the average particle size of crystal (d) base on coherent diffraction domain size was estimated using the Scherrer Equation (5) and XRD data [40]:

$$d = \frac{K\lambda}{\beta\cos(\theta)}, \tag{5}$$

where β is FWHM (Full Width at Half Maximum, in radians) from the diffraction peak, approximated for Cu *K*α and instrument widening, and *K* is a constant with a magnitude that depends on the crystal form factor, referred to as the diffraction (hkl) plane. The actual *K* varies from 0.62 to 2.08, while the commonly used value is 0.94 assuming β is FWHM, and the Integral Breadth is 0.89 [41]. Meanwhile, λ is the wavelength of the used X-rays, λCu is 0.1540598 Å, and θ is the diffraction angle [42].

3. Results and discussion

3. 1. Scanning Electron Microscope (SEM) image and particle distribution graph results to the MA Mechanical Alloying (MA) product mixtures

There were 5 variations of milling time realized during the mixing process of the powdered material constituents of AMCs using the Mechanical Alloying (MA) method, namely 0.5, 6, 24, 48, and 96 hours. The dimensions and shapes characterization of the powdered materials for each sample produced from the MA process is shown in the SEM image, **Fig. 3, *a*, 4, *a*, 5, *a*, 6, *a*, 7, *a***. Whereas, the constituent AMCs powders from the MA process were measured using the PSA Cilas 1090 Machine. The PSA measurement results are shown in **Fig. 3, *b*, 4, *b*, 5, *b*, 6, *b*, 7, *b*.** This method of coding is based on the milling time variables of 0.5 hours, 6 hours, 24 hours, 48 hours, and 96 hours shown in **Fig. 3, *a*, 4, *a*, 5, *a*, 6, *a*, 7, *a*** and codified as MA-0.5h, MA-6h, MA-24h, MA-48h, and MA-96h respectively.

The difference between the two specimens, as shown in **Fig. 3–5,** it is clear that the difference in milling time has shown differences in the shape and size of the MA powder, the longer MA milling time the smaller the powder size.

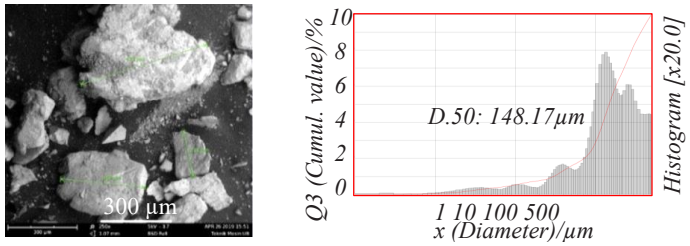

a *b*

Fig. 3. Characterization Sample of 0.5 hours Mechanical Alloying (MA-0.5 h): *a* – Scanning Electron Microscope (SEM) image; *b* – Graph of Particle Size Analyzer (PSA) measurement results

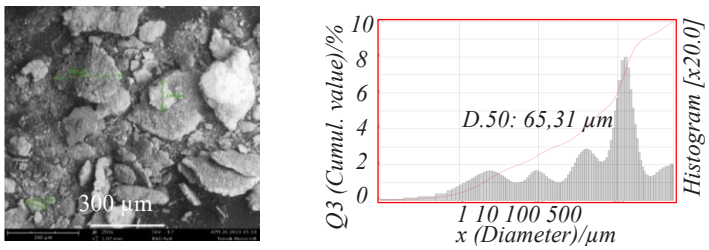

a *b*

Fig. 4. Characterization Sample of 6 hours Mechanical Alloying (MA-6h): *a* – Scanning Electron Microscope (SEM) image; *b* – Graph of Particle Size Analyzer (PSA) measurement results

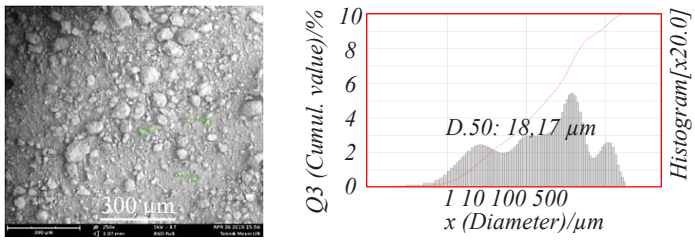

a *b*

Fig. 5. Characterization Sample of 24 hours Mechanical Alloying (MA-24h): *a* – Scanning Electron Microscope (SEM) image; *b* – Graph of Particle Size Analyzer (PSA) measurement results

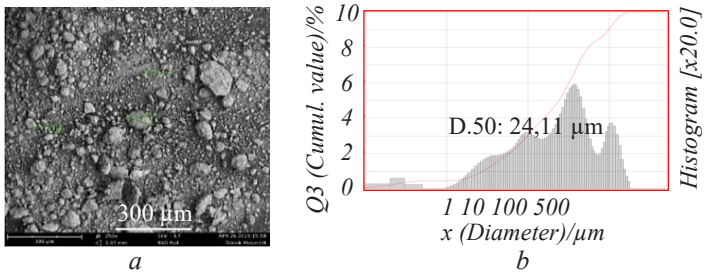

a *b*

Fig. 6. Characterization Sample of 48 hours Mechanical Alloying (MA-48h): *a* – Scanning Electron Microscope (SEM) image; *b* – Graph of Particle Size Analyzer (PSA) measurement results

Fig. 6, 7 below inform that increasing MA milling time no longer decreases powder size, but increases powder size. This condition occurs because the increase in the milling time of the MA process and powder agglomeration due to cold-weld.

Based on the images shown in **Fig. 3, *a*, 4, *a*, 5, *a*, 6, *a*, 7, *a*** it is evident that the higher the milling time applied, the smaller the particle size. This corresponds to the PSA measurement

shown in **Fig. 3, *b*, 4, *b*, 5, *b*, 6, *b*, 7.** Furthermore, supposing this is observed between **Fig. 1, 3, *a*, 4, *a*, 5, *a*, 6, *a*, 7, *a***, the difference is clear.

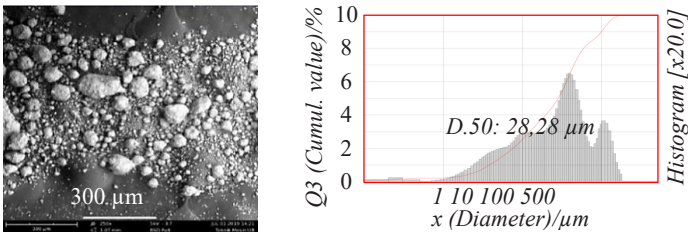

a *b*

Fig. 7. Characterization Sample of 96 hours Mechanical Alloying (MA-96h): *a* – Scanning Electron Microscope (SEM) image; *b* – Graph of Particle Size Analyzer (PSA) measurement results

In **Fig. 1,** the powder form tends to be complex with a sharp surface. On the contrary, from **Fig. 3, *a*, 4, *a*, 5, *a*, 6, *a*, 7, *a,*** the powder mixture image produced by MA show that its form tends to be blunt with relatively lesser surface roughness and radius which indicate the occurrence of cold-weld.

3. 2. X-ray Diffraction (XRD) characterization and particle size analysis of cold-weld produced by Mechanical Alloying (MA)

Besides using the PSA Cilas 1090 instrument, the cold-weld powder produced by the MA process was also measured using an X-Ray Diffraction Tool. XRD measurement results are shown in **Fig**. **8.** The milling time parameter applied is 0.5 to 96 hours, aimed to determine the phase change that occurs. It was observed that the phase graphs from MA-0.5 h to MA-96h in **Fig**. **8** have similar shapes and features, and slightly high intensities [43]. This difference is presumed to be influenced by several impurities contained in the constituent materials of AMCs powder, such as FeO_2, ZrO_2, and TiO_2, which have relatively small % wt. The dominant phase with the highest intensity is aluminium, followed by SiO_2.

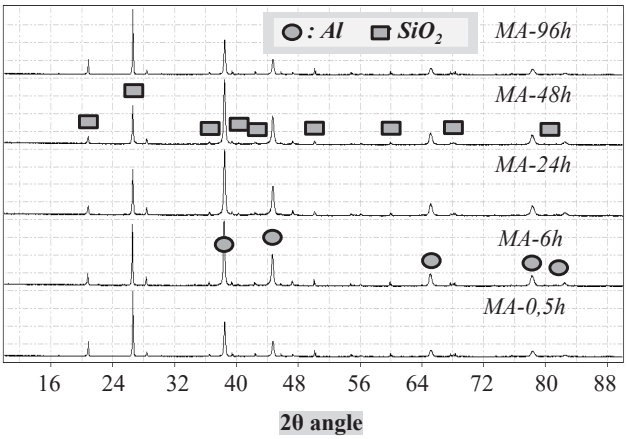

Fig. 8. X-ray Diffraction (XRD) pattern phases for Mechanical Alloying (MA) results based on different milling times

The XRD data for MA cold-weld powder was used to calculate the poly-crystal size using the Scherrer equation. The calculations proved that there is a tendency for the particle size to get smaller along with the increasing milling time, as shown in **Fig. 9**. Initially, the mixed powdered material size was 219.78 nanometers, after the application of a milling time of 0.5 hours. However, it continued to decrease to 140.47 nanometers after the application of milling time of 96 hours. Initially, the measured cold-weld powder using the PSA Cilas 1090 instrument was D50: 148.17 µm

for MA-0.5h, which decreased to D50: 18.17 μm for MA-24h, and slightly increased to D50: 24.11 μm for MA-48h and D50: 28.28 μm for MA-96h. The trend line of the test for cold-welds powder size using PSA-1090 was calculated by the Scherrer equation shown in **Fig**. **9**, which has similar tendencies irrespective of the fact that a different measurement method was adopted.

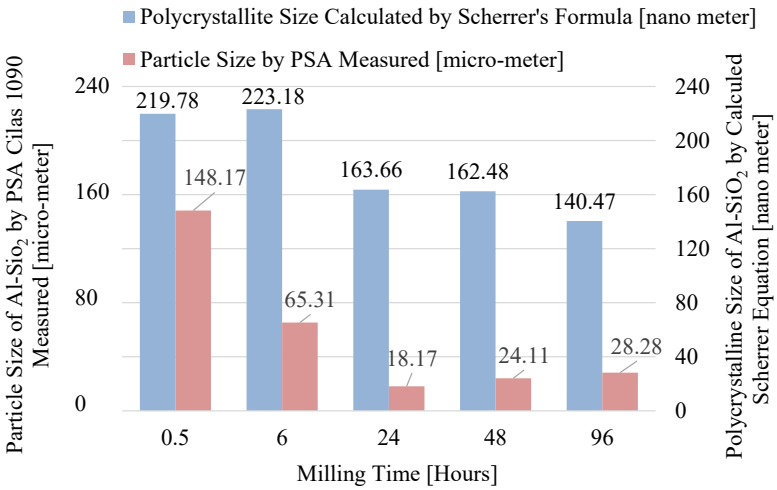

Fig. 9. Particle Size Chart of Cold-weld Produced by Mechanical Alloying (MA)

Fig. 9 indicates that initially, the particle size of the material from the mechanical alloying process decreases rapidly, then slowly. Although, at specific sizes, it increases slightly due to clots during the cold-weld cycle. However, assuming the milling time continues to increase, the particle size tends to decrease. Furthermore, when collision and the cold-welding process occur, the material coagulates and increases in size, then the powder size decreases again. This trend occurs because the constituent powders for the manufacture of AMCs consist of ductile and brittle materials namely aluminium and silica sand respectively. During the MA process with radial ball mill, several techniques including collisions, deformations, cold-welds, and particle fracture that repeatedly occurred continuously and simultaneously till a specific milling time were reached [9].

3. 3. Porosity analysis

The theoretical density of AMCs constituent powder, specimens, and the porosity were respectively determined using equations (2)–(4). Furthermore, the calculated porosity results are shown in **Fig. 10**.

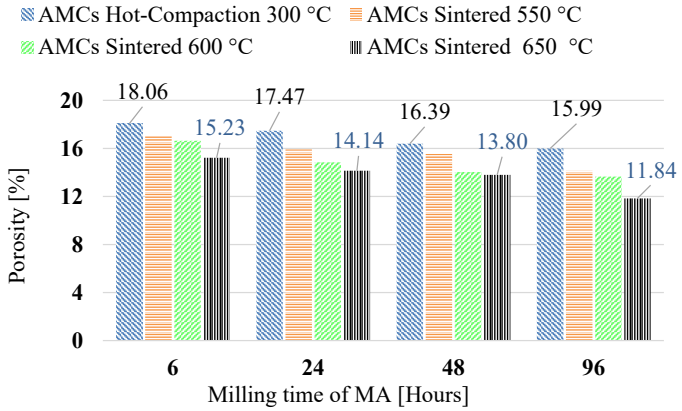

Fig. 10. Histogram of porosity of the Aluminium Matrix Composites (AMCs) specimen the difference in Mechanical Alloying (MA) milling time and sintering temperature

Based on the graph in **Fig. 6**, it is clear that AMCs porosity after the sintering process shows a decrease of approximately 40.8 %, where the initial value for AMCs-6h in the Green Hot-Compaction 300 °C sample is 18.06 %, which further reduced to 11.84 % in AMCs-96 h samples at 650 °C. An increase in the applied MA milling time causes an increase in the powder that diffuses from the matrix and reinforced particles as well as the cold-weld density and decreases the AMCs' porosity. Similarly, an increase in sintering temperature, during hot compaction causes the matrix particles to rapidly turn into semi-solid, as well as increases the wetting properties of the matrix and increasingly fills the gaps with smaller particles.

3. 4. Characterization and Microstructure Analysis of Aluminium Matrix Composites (AMCs) Product

3. 4. 1. X-ray Diffraction (XRD) analysis

AMCs specimens, using cold welding powder resulting from the MA process, were further processed during hot solidification and followed by a sintering technique. It is assigned an additional unique code associated with Bulk Sintering, abbreviated as BS, followed by MA time. Therefore, AMCs specimens using an MA time of 6 hours and processed at a sintering temperature of 600 °C were assigned a unique code of BS-6h-600 °C. This unique codification is applied to the entire specimen, as shown in **Fig. 11**, which includes BS-6h-650 °C, BS-24 h-550 °C, BS-24 h-600 °C, BS-48h-550 °C, BS-48 h-600 °C BS-96h-550 °C, and BS-96h-600 °C.

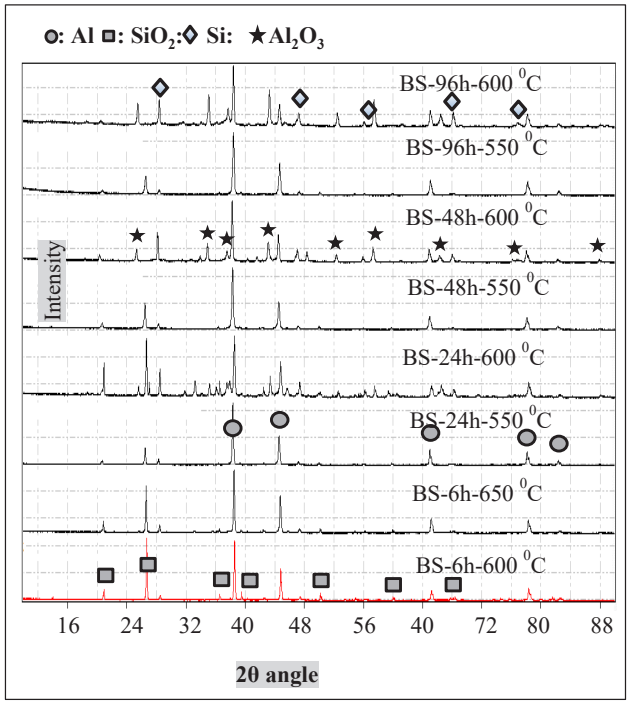

Fig. 11. X-ray Diffraction (XRD) phase patterns for AMCs-BS specimens with different milling times and different sintering temperatures

The XRD pattern result shown in **Fig. 11** was observed and analyzed, especially on BS-24 h-600 °C, BS-48h-600 °C, and BS-96h-600 °C specimens. It is clear that the longer the MA milling time and the higher the applied sintering temperature causes an increase in the intensity of the Alumina and Si phases. On the contrary, SiO_2 and Al intensity tend to decrease. This shows the formation of excess compounds and the significant increase in the concentration of Alumina and Si phases. This indicates that the transformation of aluminium and silica to form an alumina phase occurred at a temperature of 600 °C. Conversely, for AMCs, which was subjected to the MA process for 6 hours, even though it was sintered at 650 °C, the BS-6h-650 °C specimen did not show any alumina phase transformation. Likewise, AMCs use a cold-weld powder with MA 24h, 48h,

and 96 h, while the sintering temperature is reduced to 550 °C, therefore it also does not exhibit the expected alumina transformation.

3. 4. 2. SEM-EDX Scanning Electron Microscope – Energy Dispersive X-Ray Spectroscopy (SEM-EDX) analysis

Fig. 12–15 shows the microstructure SEM-EDX of the BS-6h-650 °C specimen, BS-24 h-600 °C, BS-48h-600 °C, and BS-96h-600 °C respectively. The distribution of the elements characterizing the results using SEM-EDX for each sample is shown and placed to the right of the image of each sample's, including the 4 elements with the highest percentage, namely Aluminum (Al), Silicon (Si), Iron (Fe), and Oxygen (O). In the SEM-EDX **Fig. 12**, the particle size is relatively coarse and excessively porous. There is a visible agglomeration of several phases and an invisible formation of the Al_2O_3, which is indicated by the grain boundaries in the form of fractures separating the Al and O elements, however, a small part was found.

Fig. 13, 14 shows that the particle size of AMCs microstructure with MA milling times of 24 hours and 48 hours is relatively smaller. After undergoing the sintering process at a temperature of 600 °C, a stroke pattern was formed between elements Al and O at a relatively similar position, possibly in the Al_2O_3 phase. However, the phase clumps are apparent, indicating that the homogeneity of the mixture is poor. It is slightly porous, and the particle size is finer than the BS-6h specimen.

In contrast, the Al phases in the BS-96h-600 °C specimen microstructure in **Fig. 15** appear to be evenly distributed, indicating a homogeneous mixture compared to the others. The Al_2O_3 phase is likely to form, as indicated by the relative distribution of the Al and O elements. Nevertheless, porosity is quite significant because finer powder leads to easier agglomerate. However, **Fig. 12** indicate the agglomeration of much smaller particle sizes has stronger bonds than in coarse-sized AMCs-6h-650 °C specimens. This porosity is also caused by the presence of some impurities such as Zn, which has a lower boiling point than Al and starts to burn, thereby leading to cracks in the grain boundary area. The presence of trapped air is due to the rapid cooling of the external air.

In addition to the decreased MA material clumping and increased homogeneity, the composite product's density also increases due to the increased milling time applied. Sample porosity values are AMCs with codes 6h-650 °C, BS-24 h-650 °C, BS-48 h-650 °C, and BS-96 h-650 °C is 15.23 %, 14.14 %, 13.80 %; and 11.84 gram/cm^3 respectively.

Based on these SEM-EDX characterizations in **Fig. 12–15,** it is evident that AMCs specimens from MA and sintering are relatively similar to the results of XRD analysis.

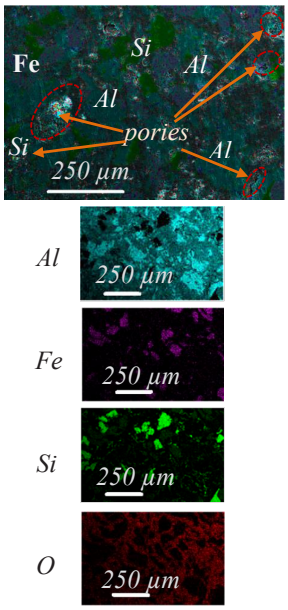

Fig. 12. Scanning Electron Microscope – Energy Dispersive X-ray (SEM-EDX) for Mechanical Alloying 6 hours and 650 °C Sintered Specimen (BS-6h-650 °C)

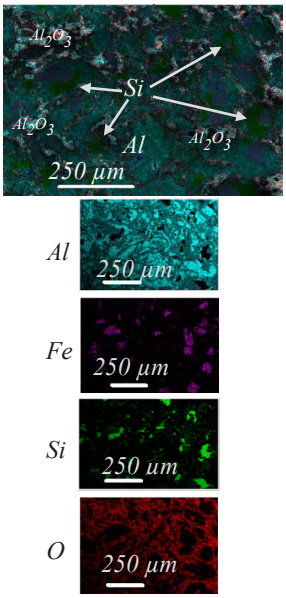

Fig. 13. Scanning Electron Microscope – Energy Dispersive X-ray (SEM-EDX) for Mechanical Alloying 24 hours and 600 °C Sintered Specimen (BS-24h-600 °C)

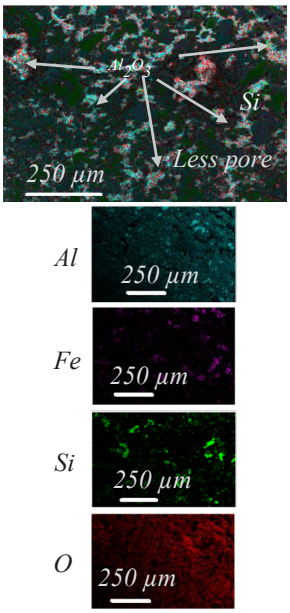

Fig. 14. Scanning Electron Microscope – Energy Dispersive X-ray (SEM-EDX) for Mechanical Alloying 48 hours and 600 °C Sintered Specimen (BS-48h-600 °C)

The longer the milling time parameters are applied, the phase shift of aluminium and SiO_2 or other oxides becomes clearer, which indicates their occurrences. The second phase transformation is alumina at a sintered temperature that is relatively lower than that of the normal reaction, 600 °C.

According to the above analysis, it proves that the MA process has resulted in cracks and fractures in the powder, interstitials and substitutions occur between particles in the lattice, the powder size is getting smaller so that the absorption of heat energy increases. This situation caused the initiation of anion and cation pairs in cold-weld alloys to occur, reinforcing powders is more evenly distributed in the matrix [9]. This condition has triggered a phase transformation from aluminium and silica to alumina when sintering processed, following the reaction equation (6) under the normal reaction temperature, 1000 to 1300 °C [18].

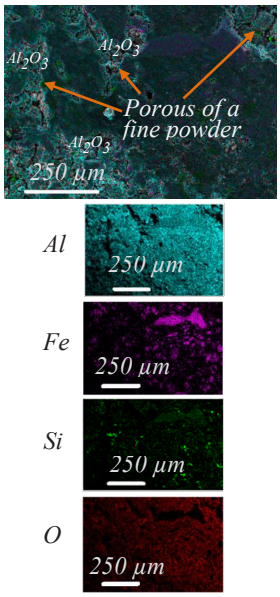

Fig. 15. Scanning Electron Microscope – Energy Dispersive X-ray (SEM-EDX) for Mechanical Alloying 96 hours and 600 °C Sintered Specimen (BS-96h-600 °C)

However, this experimental research will only be successful if the MA process parameters are applied optimally with a minimum milling time of 24 hours and a minimum sintering temperature of 600 °C:

$$4Al+3SiO_2 \rightarrow 3Si+2Al_2O_3. \quad (6)$$

Based on this study results, where this experiment has resulted in a second phase transformation of alumina at a relatively low temperature from normal reaction, so it can be recommended as a friction brake material, because in addition to alumina being harder than the SiO_2 reinforcement used, theoretically its wear resistance also increases [16, 18]. The development of this research is to obtain Non-asbestos friction brake material which is more environmentally friendly and safe against lung disease which is very dangerous.

4. Conclusions

Based on the characterization results of AMCs specimens reinforced with silica sand tailings, which includes particle-size, and XRD testing, the calculated particle size using the Scherrer equation, and microstructure testing using SEM-EDX, the following conclusions were made:

a) the AMCs powder metallurgy fabrication using materials such as Al-ZnSiFeCuMg, recycled aluminium waste, reinforced with silica sand tailings was successfully mixed using the MA technology;

b) the mixing of AMCs constituent powders using the MA process was proven to successfully and properly crush the composites' powder. The more milling time applied, the more evenly distributed the reinforced powder is on the matrix, and the more the homogeneous mixture. Therefore, the initial process of MA is imperative in powder metallurgy technology;

c) measurement of powder from the MA process using the PSA Cilas 1090 instrument showed that the milling time parameters increase leading to a decrease in particle size tending and a slight increase. Likewise, when the crystal particle size of the MA sample was calculated using the Scherrer equation of the XRD data, the result showed a similar linear trend with decreasing values;

d) MA milling time of 6h and sintering temperature of approximately 650 °C for AMCs specimens reinforced with silica tailings sand did not occur an alumina phase transformation reaction. The new Al_2O_3 transformation occurred when a minimum of 24 hours milling time was applied with a minimum sintering temperature of 600 °C, in BS-24h-600 °C, BS-48-600 °C, and

BS-96-600 °C specimens. In addition, the temperature of this transformation reaction is lesser than the normal one, which is relatively 1000 to 1300 °C.

Acknowledgement

This work was supported by the Scholarship for Leading Indonesian Lecturers – Domestic Education (BUDI-DN) and the Indonesia Endowment Fund for Education (LPDP) under grant number PRJ-6506/LPDP.3/2016 as well as grants from Corporate Social Responsibility (CSR) Pt. Timah Tbk. Number: 69/ST. PTTIMAH/2019.

References

[1] Garg, P., Jamwal, A., Kumar, D., Sadasivuni, K. K., Hussain, C. M., Gupta, P. (2019). Advance research progresses in aluminium matrix composites: manufacturing & applications. Journal of Materials Research and Technology, 8 (5), 4924–4939. doi: https://doi.org/10.1016/j.jmrt.2019.06.028

[2] Ceschini, L., Dahle, A., Gupta, M., Jarfors, A. E. W., Jayalakshmi, S., Morri, A. et. al. (2017). Mechanical Behavior of Al and Mg Based Nanocomposites. Engineering Materials, 95–137. doi: https://doi.org/10.1007/978-981-10-2681-2_4

[3] Vu Viet, Q., Thu, T. V. T., Duong, N. N., Ngoc, B. D., Duc, H. T. (2020). Research on the manufacturing magnesium from thanhhoa dolomite by pidgeon process. EUREKA: Physics and Engineering, 6, 97–107. doi: https://doi.org/10.21303/2461-4262.2020.001383

[4] Chaubey, A., Konda Gokuldoss, P., Wang, Z., Scudino, S., Mukhopadhyay, N., Eckert, J. (2016). Effect of Particle Size on Microstructure and Mechanical Properties of Al-Based Composite Reinforced with 10 Vol.% Mechanically Alloyed Mg-7.4 % Al Particles. Technologies, 4 (4), 37. doi: https://doi.org/10.3390/technologies4040037

[5] Allazadeh, M. R., Balazsi, C. (2013). Reinforced Aluminum Matrix Composite Application in Friction Material. Recent Patents on Corrosion Science, 3 (1), 39–46. doi: https://doi.org/10.2174/2210683911202999006

[6] Schmidt, A., Siebeck, S., Götze, U., Wagner, G., Nestler, D. (2018). Particle-Reinforced Aluminum Matrix Composites (AMCs) – Selected Results of an Integrated Technology, User, and Market Analysis and Forecast. Metals, 8 (2), 143. doi: https://doi.org/10.3390/met8020143

[7] El-Eskandarany, M. S. (2015). The history and necessity of mechanical alloying. Mechanical Alloying, 13–47. doi: https://doi.org/10.1016/b978-1-4557-7752-5.00002-4

[8] Jamal, N. A., Farazila, Y., Ramesh, S., Anuar, H. (2014). Role of mechanical alloying parameters on powder distribution of Al/Cu alloy and Al/Cu composite. Materials Research Innovations, 18, S6-190–S6-195. doi: https://doi.org/10.1179/1432891714z.000000000956

[9] Suryanarayana, C. (2019). Mechanical Alloying: A Novel Technique to Synthesize Advanced Materials. Research, 2019, 1–17. doi: https://doi.org/10.34133/2019/4219812

[10] Nová, K., Novák, P., Průša, F., Kopeček, J., Čech, J. (2018). Synthesis of Intermetallics in Fe-Al-Si System by Mechanical Alloying. Metals, 9 (1), 20. doi: https://doi.org/10.3390/met9010020

[11] Suñol, J.-J. (2021). Mechanical Alloying: Processing and Materials. Metals, 11 (5), 798. doi: https://doi.org/10.3390/met11050798

[12] Koch, C. C., Scattergood, R. O., Youssef, K. M., Chan, E., Zhu, Y. T. (2010). Nanostructured materials by mechanical alloying: new results on property enhancement. Journal of Materials Science, 45 (17), 4725–4732. doi: https://doi.org/10.1007/s10853-010-4252-7

[13] Martinez Ruiz, M., Rivera Olvera, J. N., Morales Davila, R., González Reyes, L., Garibay Febles, V., Garcia Martinez, J., Diaz Barriga Arceo, L. G. (2020). Synthesis and Characterization of Mechanically Alloyed, Nanostructured Cubic MoW Carbide. Applied Sciences, 10 (24), 9114. doi: https://doi.org/10.3390/app10249114

[14] Caballero, E., Cuevas, F., Ternero, F., Astacio, R., Montes, J., Cintas, J. (2018). In Situ Synthesis of Al-Based MMCs Reinforced with AlN by Mechanical Alloying under NH3 Gas. Materials, 11 (5), 823. doi: https://doi.org/10.3390/ma11050823

[15] Balcı, Ö., Prashanth, K., Scudino, S., Ağaoğulları, D., Duman, İ., Öveçoğlu, M. et. al. (2015). Effect of Milling Time and the Consolidation Process on the Properties of Al Matrix Composites Reinforced with Fe-Based Glassy Particles. Metals, 5 (2), 669–685. doi: https://doi.org/10.3390/met5020669

[16] Suryanarayana, C., An, I.-S. (2006). Mechanical Alloying and Milling. Journal of Korean Powder Metallurgy Institute, 13 (5), 371–372. doi: https://doi.org/10.4150/kpmi.2006.13.5.371

[17] Yu, P., Deng, C.-J., Ma, N.-G., Ng, D. H. L. (2004). A new method of producing uniformly distributed alumina particles in Al-based metal matrix composite. Materials Letters, 58 (5), 679–682. doi: https://doi.org/10.1016/j.matlet.2003.06.001

[18] Woo, K. D., Lee, H. B. (2007). Fabrication of Al alloy matrix composite reinforced with subsive-sized Al2O3 particles by the in situ displacement reaction using high-energy ball-milled powder. Materials Science and Engineering: A, 449-451, 829–832. doi: https://doi.org/10.1016/j.msea.2006.02.402

[19] Karbasi, M., Razavi, M., Taheri, M., Vashaee, D., Tayebi, L. (2013). Preparation of Al-SiC-Al2O3 metal matrix composite powder by mechanochemical reaction between Al, SiO2 and C. Micro & Nano Letters, 8 (9), 519–522. doi: https://doi.org/10.1049/mnl.2013.0419

[20] Böer, K. W., Pohl, U. W. (2015). Crystal Defects. Semiconductor Physics, 1–51. doi: https://doi.org/10.1007/978-3-319-06540-3_15-1

[21] Suezawa, M., Iijima, Y., Yonenaga, I. (2017). On the nature of thermal equilibrium point defects in Si: Are the thermal equilibrium point defects in Si crystals Frenkel pairs or Schottky defects? Japanese Journal of Applied Physics, 56 (4), 048005. doi: https://doi.org/10.7567/jjap.56.048005

[22] Casati, R., Vedani, M. (2014). Metal Matrix Composites Reinforced by Nano-Particles – A Review. Metals, 4 (1), 65–83. doi: https://doi.org/10.3390/met4010065

[23] Armstrong, R. (2019). Dislocation Mechanics Pile-Up and Thermal Activation Roles in Metal Plasticity and Fracturing. Metals, 9 (2), 154. doi: https://doi.org/10.3390/met9020154

[24] Fogagnolo, J. B., Ruiz-Navas, E. M., Robert, M. H., Torralba, J. M. (2003). The effects of mechanical alloying on the compressibility of aluminium matrix composite powder. Materials Science and Engineering: A, 355 (1-2), 50–55. doi: https://doi.org/10.1016/s0921-5093(03)00057-1

[25] Azarniya, A., Azarniya, A., Abdollah-zadeh, A., Madaah Hosseini, H. R., Ramakrishna, S. (2019). In Situ Hybrid Aluminum Matrix Composites: A Review of Phase Transformations and Mechanical Aspects. Advanced Engineering Materials, 21 (7), 1801269. doi: https://doi.org/10.1002/adem.201801269

[26] Fuad, A., Mufti, N., Diantoro, M. et. al. (2016). Synthesis and characterization of highly purified nanosilica from pyrophyllite ores. AIP Conference Proceedings. doi: https://doi.org/10.1063/1.4943715

[27] Brough, D., Jouhara, H. (2020). The aluminium industry: A review on state-of-the-art technologies, environmental impacts and possibilities for waste heat recovery. International Journal of Thermofluids, 1-2, 100007. doi: https://doi.org/10.1016/j.ijft.2019.100007

[28] Sukanto, Soenoko, R., Suprapto, W., Irawan, Y. S. (2020). Characterization of aluminium matrix composite of Al-ZnSiFeCuMg alloy reinforced with silica sand tailings particles. Journal of Mechanical Engineering and Sciences, 14 (3), 7094–7108. doi: https://doi.org/10.15282/jmes.14.3.2020.11.0556

[29] Sivakumar, S., Teow, H. L., Singh, R., Niakan, A., Mase, N. (2016). The Effect of Iron Oxide on the Mechanical and Ageing Properties of Y-TZP Ceramic. Key Engineering Materials, 701, 225–229. doi: https://doi.org/10.4028/www.scientific.net/kem.701.225

[30] Huo, S. H., Qian, M., Schaffer, G. B., Crossin, E. (2011). Aluminium powder metallurgy. Fundamentals of Aluminium Metallurgy, 655–701. doi: https://doi.org/10.1533/9780857090256.3.655

[31] Zuhailawati, H., Samayamutthirian, P., Mohd Haizu, C. H. (2007). Fabrication of low cost of aluminium matrix composite reinforced with silica sand. Journal of Physical Science, 18 (1), 47–55. Available at: https://jps.usm.my/wp-content/uploads/2014/11/Article-18-1-5.pdf

[32] Mohan, S., Gautam, G., Kumar, N., Gautam, R. K., Mohan, A., Jaiswal, A. K. (2016). Dry sliding wear behavior of Al-SiO_2 composites. Composite Interfaces, 23 (6), 493–502. doi: https://doi.org/10.1080/09276440.2016.1149363

[33] Munasir, Triwikantoro, Zainuri, M., Bäßler, R., Darminto (2019). Mechanical strength and corrosion rate of aluminium composites (Al/SiO_2): Nanoparticle silica (NPS) as reinforcement. Journal of Physical Science, 30 (1), 81–97. doi: https://doi.org/10.21315/jps2019.30.1.7

[34] Sukanto, Soenoko, R., Suprapto, W., Irawan, Y. S. (2019). Parameter Optimization of Ball Milling Process for Silica Sand Tailing. IOP Conference Series: Materials Science and Engineering, 494, 012073. doi: https://doi.org/10.1088/1757-899x/494/1/012073

[35] Ubenthiran, S., Thanihaichelvan, M., Singh, R. (2018). Effect of Air and Argon Sintering Atmospheres on Properties and Hydrothermal Aging Resistance of Y-TZP Ceramics. Journal of Materials Engineering and Performance, 27 (7), 3574–3580. doi: https://doi.org/10.1007/s11665-018-3428-1

[36] Wahyudie, I. A., Soenoko, R., Suprapto, W., Irawan, Y. S. (2020). Enhancing hardness and wear resistance of $ZrSiO_4$-SnO_2/Cu10Sn composite produced by warm compaction and sintering. Metalurgija, 59 (1), 27–30. Available at: https://hrcak.srce.hr/file/327708

[37] Tian, T., Hao, Z., Li, X., Jia, C., Peng, S., Zhu, Q., Ge, C. (2020). Influence of aging treatment on microstructure and properties of a novel spray formed powder metallurgy superalloy FGH100L. Journal of Alloys and Compounds, 830, 154699. doi: https://doi.org/10.1016/j.jallcom.2020.154699

[38] Huo, H., Woo, K. D. (2006). In situ synthesis of Al_2O_3 particulate-reinforced Al matrix composite by low temperature sintering. Journal of Materials Science, 41 (11), 3249–3253. doi: https://doi.org/10.1007/s10853-005-5476-9

[39] ASTM International – ASTM B962-13. Standard Test Methods for Density of Compacted or Sintered Powder Metallurgy (PM) Products Using Archimedes' Principle. Available at: https://standards.globalspec.com/std/3851131/astm-b962-13

[40] Hargreaves, J. S. J. (2016). Some considerations related to the use of the Scherrer equation in powder X-ray diffraction as applied to heterogeneous catalysts. Catalysis, Structure & Reactivity, 2 (1-4), 33–37. doi: https://doi.org/10.1080/2055074x.2016.1252548

[41] Horikoshi, S., Serpone, N. (2013). Introduction to Nanoparticles. Microwaves in Nanoparticle Synthesis, 1–24. doi: https://doi.org/10.1002/9783527648122.ch1

[42] Muniz, F. T. L., Miranda, M. A. R., Morilla dos Santos, C., Sasaki, J. M. (2016). The Scherrer equation and the dynamical theory of X-ray diffraction. Acta Crystallographica Section A Foundations and Advances, 72 (3), 385–390. doi: https://doi.org/10.1107/s205327331600365x

[43] Wang, J. (2008). Mechanical alloying of amorphous Al–SiO_2 powders. Journal of Alloys and Compounds, 456 (1-2), 139–142. doi: https://doi.org/10.1016/j.jallcom.2007.02.027

Received date 23.09.2021
Accepted date 14.12.2021
Published date 10.01.2022

How to cite: *Sukanto, Suprapto, W., Soenoko, R., Irawan, Y. S. (2022). The effect of milling time on the alumina phase transformation in the AMCs powder metallurgy reinforced by silica-sand-tailings. EUREKA: Physics and Engineering, 1, 103–117. doi: https://doi.org/10.21303/2461-4262.2022.001906*